THE SURFACE OF ASTEROID 951 GASPRA

PHILIP J. STOOKE
Department of Geography, University of Western Ontario, London, Ontario, Canada N6A 5C2

(Received 17 December, 1996; Accepted 14 January, 1997)

Abstract. I present new maps, photomosaics and geological interpretations of asteroid 951 Gaspra. Facets and limb concavities suggest a long history of large impacts producing 5 to 7 km diameter craters. Craters 1 to 4 km in diameter date the last facet-forming impact, though it is not clear which facet this formed. These craters are more numerous than previously thought because much of the area seen at high resolution seems to be depleted in these larger craters. Craters in that area probably date the last body-jolting impact. Linear features, probably the surface expressions of deep fractures, form at least two groups with different trends and probably different ages. Previously noted fresh and spectrally distinct materials are concentrated on ridges. One or two dark markings occur on a steep slope seen at high sun. Smooth materials, probably consisting of thicker or more mobile regolith than elsewhere, occur on steep slopes, usually on rotational leading surfaces.

Key words: Asteroids, morphology.

1. Introduction

Asteroid 951 Gaspra was observed by the Galileo spacecraft on 29 October 1991, the first asteroid encounter by a spacecraft. Fifty-seven images containing Gaspra data were returned from the spacecraft (Veverka et al., 1994a), revealing an angular object with rounded edges, small craters, larger facets of controversial origin, and long narrow depressions referred to as grooves (Veverka et al., 1994b). The images, comprising 12 useful views of Gaspra, were used by Thomas et al. (1994) to derive a shape model and simple maps of surface features.

In this paper I present more detailed maps and photomosaics of the surface of Gaspra, and geological interpretations of features seen in the images. Super-resolution composites of some images from multi-spectral sequences were used to improve or raise confidence in geological interpretations. The mapping methods used here were described by Stooke (in press), Stooke and Lumsdon (1993) and references in those papers and are not reiterated in detail here.

2. Data

Representative Gaspra images are shown in Figure 1, and the viewing and illumination geometry is described in Table I. All Galileo images in this paper are identified according to their file names on the Planetary Data System CD-ROM GO-0007. In Table I the first six-digit number is the subdirectory name, and the final four-digit number is the file name. Veverka et al. (1994a) give more complete

Earth, Moon and Planets **75**: 53–75, 1997.

Table I
Galileo image sequences for 951 Gaspra

Image Number	Spacecraft lat/long	Sub-solar lat/long	Phase angle	Pixel size (km)
010728 5600	37, 131	5, 118	34	1.66
010728 9100	37, 161	5, 148	34	1.49
010729 2600-2745	37, 193	5, 180	34	1.31
010729 6100	37, 222	5, 208	34	1.15
010729 9600	37, 252	5, 238	35	0.97
010730 3100-3245	38, 284	5, 270	35	0.79
010730 6600	38, 313	5, 299	35	0.63
010731 0100	38, 343	5, 329	36	0.46
010731 3539-3865	40, 16	5, 1	37	0.273
010731 4900-5100	41, 26	5, 10	38	0.214
010731 5839-6339	42, 36	5, 21	39	0.163
010731 8313-8326	52, 64	5, 40	51	0.054

information on Galileo images. All images in Figure 1 were processed in the same way. Raw images were enlarged by pixel replication. They were contrast stretched to enhance visibility of subtle features. The stretched images were high pass filtered, and the filtered version was merged with the stretched image to provide some of the advantages of both forms of processing. This procedure has been found to maximize interpretability of the images. For the highest resolution view (Figure 1b, bottom), the two separate frames constituting the image were mosaicked before processing, resulting in some resampling of the frame covering the more pointed end of Gaspra. In all cases, interpretations were checked against raw images.

In addition, all images to which the "super-resolution" method (Cheeseman et al., 1994; Stooke, in press) could be applied were processed in this way. These images are included in a companion paper (Stooke, P.J., "Linear Features on Asteroid 951 Gaspra", submitted to *Earth, Moon and Planets*, referred to hereafter as "Stooke, submitted paper"). Figure 2 shows the application of this method to one pair of images from the sequence 0107315839-6339. The two sharpest images of the sequence (Figure 2, top) were enlarged by a factor of 2 by pixel replication, registered to the nearest half pixel and merged. The result (Figure 2, bottom left) is easier to interpret, being less degraded by the blocky appearance of structures near the size of a single pixel. No other processing (e.g. smoothing, sharpening) has been performed on the merged image. At bottom right in that figure the highest resolution image (0107318326) is resampled at the same pixel size as the super-resolution composite. Clearly, not all detail visible at that pixel size is revealed by the super-resolution method, but no artifacts are obvious and small features are more reliably identifiable in the composite. It is particularly relevant, considering

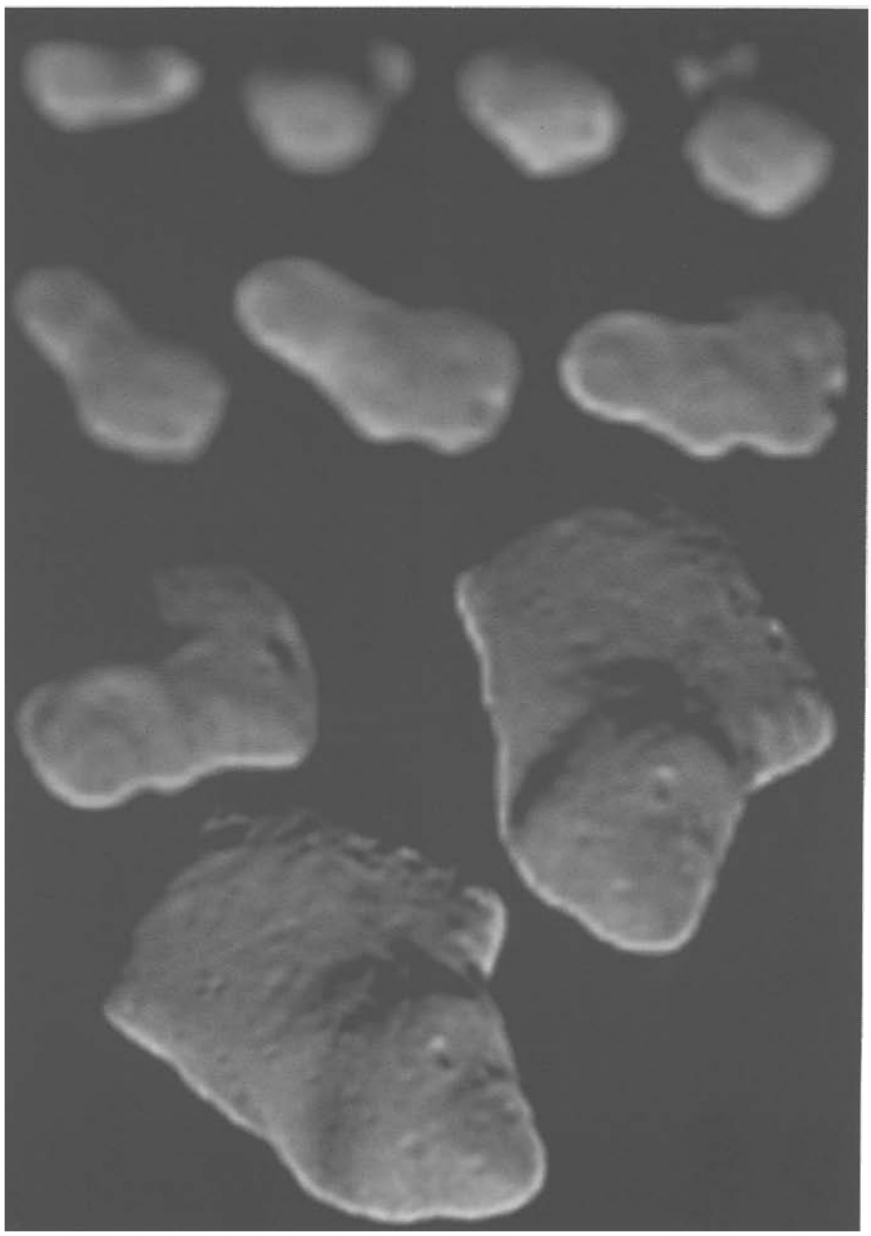

Figure 1a. (a) Galileo images of Gaspra taken during approach. Each is a composite of a contrast-stretched version and a high-pass-filtered version.

Figure 1b. (b) The two highest resolution views of Gaspra, processed as in Figure 1a.

the use of this technique to identify grooves on Hyperion (Stooke, in press), that spurious linear features have not been created.

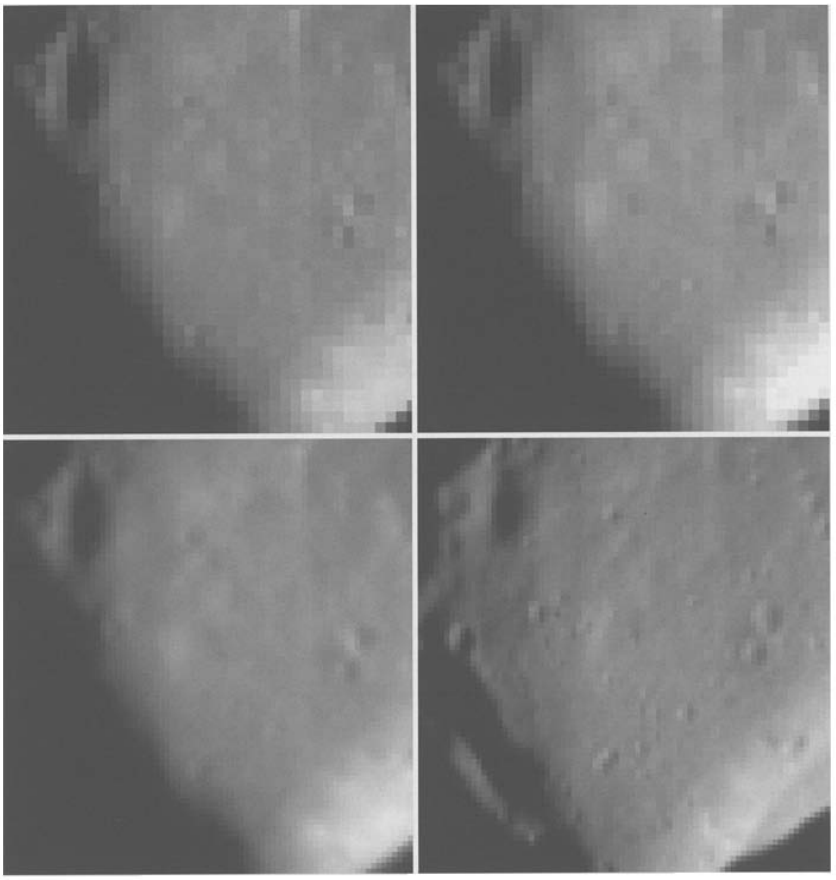

Figure 2. Parts of two images taken during sequence 0107316065-6113 (top, resolution 160 m/pixel), a super-resolution composite of the two (bottom left, geometric resolution 80 m/pixel), and part of image 0107318326 resampled to 80 m/pixel (bottom right).

3. Method

A preliminary shape model of Gaspra was prepared by digitizing the contours of the map by Thomas et al. (1994, Figure 6a) and interpolating radii to a 5° by 5° matrix. This very approximate model was refined as in previous studies (e.g. Stooke and Lumsdon, 1993; Stooke, in press) by adjusting local radii until the shape model duplicated the shapes of limbs and terminators in all 12 useful views of Gaspra. Simonelli et al. (1995) used the Thomas et al. (1994) shape model and the photometric behaviour of Gaspra as determined by Helfenstein et al. (1994) to create synthetic lightcurves. To reduce differences between these and observed lightcurves, they modified the original shape model in southern latitudes poorly

seen by Galileo. I have used synthetic images of their revised shape model to further constrain the shape presented here.

This model differs very little from that of Thomas et al. (1994), modified by Simonelli et al. (1995), as would be expected. However, some differences are present. The region forming the southern limb in the last two image sequences is further south in my model, a change which seems to reduce parallax between the latitude-longitude grid and features seen on the limb. A shallow crater forming part of Dunne Regio, on the equator at 35° W is deeper in this model than in the earlier shape. This crater did not include any of the stereoscopic control points used by Thomas et al. (1994), and the change again reduces parallax between the grid and the surface. The south polar region in the model of Thomas et al. (1994, Figure 4) contains a depression which is flattened in this model. Galileo images provide no information on this region, and the polar hollow was an artifact of modelling. Other minor differences between the models have no significance, but reflect the range of possible interpretations permitted by the limited data.

Figure 3 shows the positions of limbs and terminators on the model. Galileo was always more than 35° N of Gaspra's equator, and never saw high southern latitudes. Most limbs lie between the equator and 20° S, except where ridges at mid-southern latitudes protrude beyond the equatorial regions in views centred near the intermediate axis. Areas where several lines coincide, essentially the whole equatorial zone, are modelled most reliably, especially for the face centred on longitude 90° which was seen at higher resolution. The northern hemisphere is mostly modelled from terminator data, stereoscopic control points and efforts to minimize parallax between the latitude-longitude grid and surface features. Some attempt was made to modify topography in the model to fit ridges and craters which appear on the images but are not seen on a limb or terminator, primarily for aesthetic purposes. Small details of contours in these regions are merely suggestive of the local topography. Crater depths and ridge heights are only very rough estimates.

The limbs are located to within about one pixel in the plane of the image, and the terminators to within 2 or 3 pixels. Table I gives the relevant pixel resolutions. Uncertainties are caused by smearing, aliasing effects at the limb, and complex relief near the terminators. When the limbs are transferred to a body-fixed coordinate system for mapping their locations become uncertain by up to several tens of degrees perpendicular to the limb traces of Figure 3, increasing radius uncertainty in the model to about 200 to 300 m even in the best areas, and up to 1 km in poorly constrained regions. Relative elevations near terminators may be accurate to within 200 m in places since small variations in topography produce large changes in the shape of the terminator. Absolute radii near terminators are reliable only near limb traces, within the limits outlined above. All things considered, the shapes of the equatorial region and the area seen at high resolution are for the most part likely to be accurate to within 300 m, but other regions have uncertainties as high as 1 km.

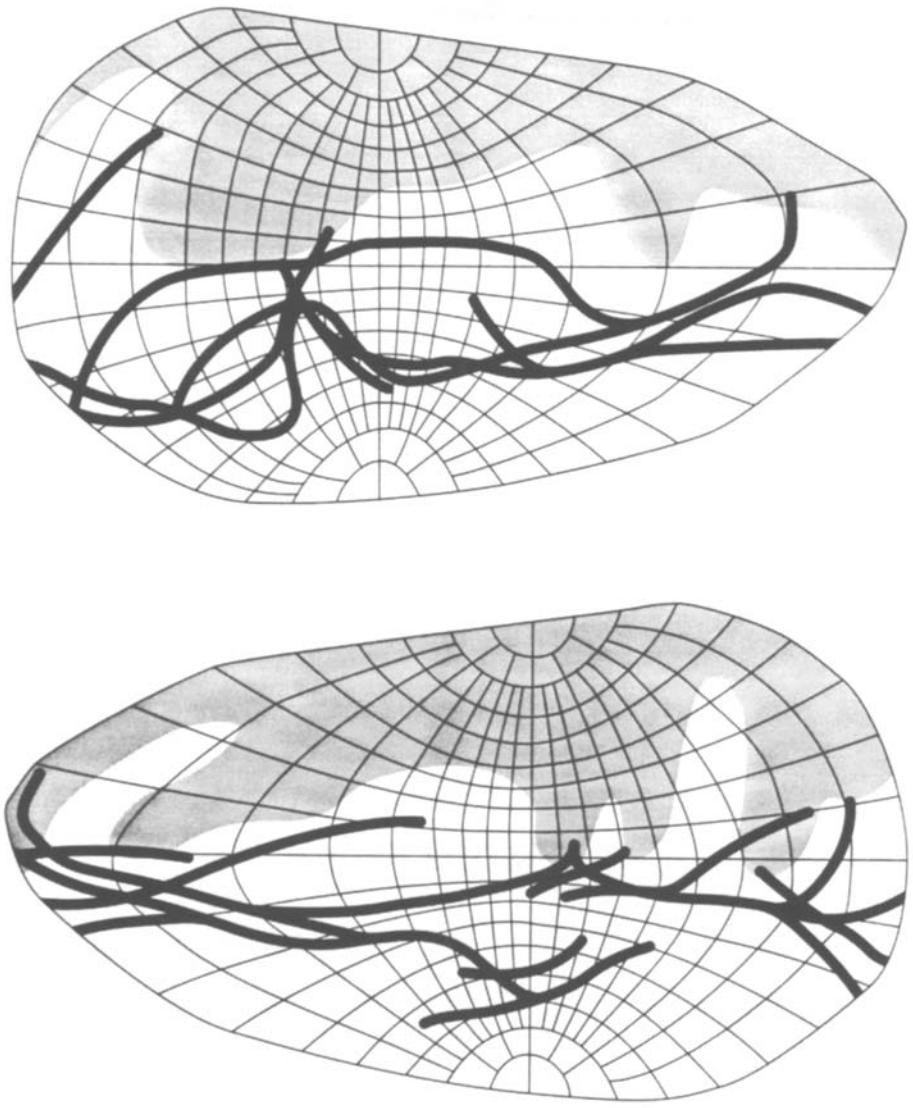

Figure 3. Locations of limbs (heavy lines) and terminators (shaded) in Galileo images.

4. The Shape of Gaspra

The topographic model is presented in Table II and illustrated in Figures 4 to 10. The original data for Table II, at the 5° spacing used during modelling, is available from the author by electronic mail or on diskette. Latitude-longitude grids corresponding to Galileo views are given in Figure 4. The rotation axes are vertical in these views regardless of the actual orientation of the asteroid in the images. Six mutually perpendicular views are presented in Figure 5.

Table II
Radii of the Gaspra shape model (km)

	Longitude									
	360	350	340	330	320	310	300	290	280	270
Latitude										
90	4.3	4.3	4.3	4.3	4.3	4.3	4.3	4.3	4.3	4.3
80	4.1	4.1	4.1	4.1	4.1	4.2	4.2	4.3	4.3	4.4
70	4.2	4.3	4.2	4.2	4.2	4.2	4.3	4.4	4.5	4.6
60	4.4	4.5	4.5	4.3	4.2	4.2	4.3	4.4	4.5	4.7
50	5.0	5.1	4.8	4.3	4.2	4.2	4.3	4.5	4.5	4.7
40	6.3	6.0	5.4	4.9	4.6	4.5	4.5	4.5	4.6	4.8
30	7.5	6.9	6.2	5.6	5.0	4.8	4.6	4.7	4.8	4.9
20	8.6	7.3	6.8	6.3	5.7	5.2	4.8	4.7	4.8	5.2
10	10.2	8.7	7.8	6.7	5.7	5.1	4.8	4.6	4.7	5.3
0	10.5	10.0	8.5	6.8	5.7	5.0	4.7	4.7	4.7	5.2
−10	9.2	9.1	8.1	6.4	5.7	5.1	4.7	4.6	4.6	4.8
−20	8.0	7.8	6.7	5.8	5.2	4.8	4.5	4.5	4.5	4.5
−30	7.0	6.6	5.7	5.1	4.8	4.6	4.4	4.4	4.4	4.4
−40	6.1	5.6	5.1	4.7	4.6	4.5	4.6	4.6	4.7	4.6
−50	5.3	5.1	4.9	4.6	4.6	4.6	4.7	4.7	4.9	4.9
−60	5.0	4.9	4.8	4.8	4.8	4.7	4.8	4.9	4.9	4.9
−70	4.8	4.8	4.7	4.7	4.7	4.7	4.7	4.7	4.7	4.8
−80	4.7	4.7	4.7	4.7	4.7	4.7	4.7	4.7	4.7	4.7
−90	4.7	4.7	4.7	4.7	4.7	4.7	4.7	4.7	4.7	4.7
	Longitude									
	270	260	250	240	230	220	210	200	190	180
Latitude										
90	4.3	4.3	4.3	4.3	4.3	4.3	4.3	4.3	4.3	4.3
80	4.4	4.4	4.4	4.4	4.4	4.4	4.4	4.5	4.5	4.5
70	4.6	4.6	4.7	4.7	4.8	4.9	4.9	5.0	5.1	5.2
60	4.7	4.9	5.0	5.1	5.2	5.3	5.4	5.5	5.7	5.9
50	4.7	5.0	5.2	5.2	5.2	5.3	5.7	5.8	6.1	6.2
40	4.8	5.0	5.2	5.5	5.4	5.5	5.9	6.1	6.5	6.8
30	4.9	5.1	5.5	5.7	5.8	6.1	6.3	6.6	7.0	7.2
20	5.2	5.5	5.8	6.0	6.2	6.3	6.4	7.1	7.3	7.4
10	5.3	6.0	6.3	6.4	6.6	6.7	7.1	7.3	7.6	7.5
0	5.2	6.3	6.7	6.8	7.0	7.2	7.3	7.4	7.7	7.6
−10	4.8	5.5	6.0	6.3	6.9	7.2	7.2	7.4	7.6	7.5
−20	4.5	4.8	5.2	5.7	6.0	6.2	6.3	6.6	6.8	7.2
−30	4.4	4.5	4.6	4.9	5.2	5.6	5.6	6.0	6.2	6.6
−40	4.6	4.6	4.6	4.7	4.8	5.0	5.3	5.5	5.8	6.2
−50	4.9	4.9	4.9	4.9	4.8	4.8	4.9	5.1	5.5	5.9
−60	4.9	4.9	4.8	4.8	4.7	4.7	4.8	4.9	5.2	5.5
−70	4.8	4.8	4.8	4.8	4.8	4.8	4.8	4.8	5.0	5.1
−80	4.7	4.7	4.7	4.7	4.7	4.7	4.8	4.8	4.8	4.8
−90	4.7	4.7	4.7	4.7	4.7	4.7	4.7	4.7	4.7	4.7

Table II
Continued

	Longitude									
	180	170	160	150	140	130	120	110	100	90
Latitude										
90	4.3	4.3	4.3	4.3	4.3	4.3	4.3	4.3	4.3	4.3
80	4.5	4.5	4.5	4.5	4.4	4.4	4.4	4.3	4.3	4.2
70	5.2	5.2	5.1	5.1	4.9	4.8	4.6	4.5	4.4	4.3
60	5.9	5.9	5.8	5.7	5.5	5.2	4.9	4.6	4.4	4.3
50	6.2	6.3	6.2	6.1	6.1	5.8	5.3	4.9	4.7	4.5
40	6.8	6.8	6.8	6.8	6.6	6.2	5.7	5.3	5.0	4.8
30	7.2	7.2	7.2	7.0	6.8	6.3	6.1	5.6	5.3	5.1
20	7.4	7.4	7.3	6.6	6.5	6.6	6.5	6.1	5.7	5.3
10	7.5	7.6	7.2	6.8	6.4	6.6	6.8	6.4	5.8	5.3
0	7.6	7.4	7.1	6.8	6.7	6.7	7.0	6.3	5.3	4.8
−10	7.5	7.4	7.0	6.8	6.6	6.7	6.6	5.8	4.9	4.4
−20	7.2	7.2	7.0	6.9	6.4	6.0	5.6	5.3	4.7	4.3
−30	6.6	6.7	6.7	6.5	5.9	5.4	5.0	5.0	4.7	4.4
−40	6.2	6.5	6.4	6.3	5.7	5.4	5.0	4.9	4.8	4.5
−50	5.9	6.1	6.2	6.2	5.8	5.4	5.0	4.9	4.7	4.6
−60	5.5	5.7	5.8	5.8	5.5	5.1	4.8	4.7	4.7	4.6
−70	5.1	5.2	5.3	5.3	5.1	4.9	4.7	4.6	4.6	4.5
−80	4.8	4.8	4.8	4.8	4.7	4.7	4.7	4.7	4.7	4.7
−90	4.7	4.7	4.7	4.7	4.7	4.7	4.7	4.7	4.7	4.7
	Longitude									
	90	80	70	60	50	40	30	20	10	0
Latitute										
90	4.3	4.3	4.3	4.3	4.3	4.3	4.3	4.3	4.3	4.3
80	4.2	4.2	4.2	4.1	4.1	4.1	4.1	4.1	4.1	4.1
70	4.3	4.2	4.1	4.1	4.0	4.0	4.1	4.1	4.1	4.2
60	4.3	4.3	4.2	4.1	4.1	4.1	4.1	4.1	4.2	4.4
50	4.5	4.5	4.4	4.3	4.4	4.4	4.6	4.8	4.9	5.0
40	4.8	4.7	4.4	4.4	4.6	4.9	5.2	5.8	6.2	6.3
30	5.1	5.0	4.8	4.8	4.8	5.2	5.8	6.9	7.4	7.5
20	5.3	5.1	5.1	5.1	5.2	5.3	6.1	7.7	8.6	8.6
10	5.3	5.1	5.1	5.1	5.3	5.3	6.1	8.0	9.8	10.2
0	4.8	4.6	4.6	4.8	5.2	5.4	6.2	8.1	9.6	10.5
−10	4.4	4.3	4.4	4.6	5.0	5.8	6.5	7.9	8.7	9.2
−20	4.3	4.2	4.3	4.5	4.9	5.8	6.4	7.2	7.6	8.0
−30	4.4	4.3	4.3	4.5	4.9	5.5	6.1	6.5	6.7	7.0
−40	4.5	4.4	4.4	4.5	4.8	5.2	5.5	5.8	6.0	6.1
−50	4.6	4.5	4.5	4.6	4.7	4.9	5.0	5.3	5.4	5.3
−60	4.6	4.6	4.6	4.6	4.7	4.7	4.8	4.9	5.0	5.0
−70	4.5	4.5	4.5	4.5	4.6	4.6	4.6	4.7	4.7	4.8
−80	4.7	4.7	4.7	4.7	4.7	4.7	4.7	4.7	4.7	4.7
−90	4.7	4.7	4.7	4.7	4.7	4.7	4.7	4.7	4.7	4.7

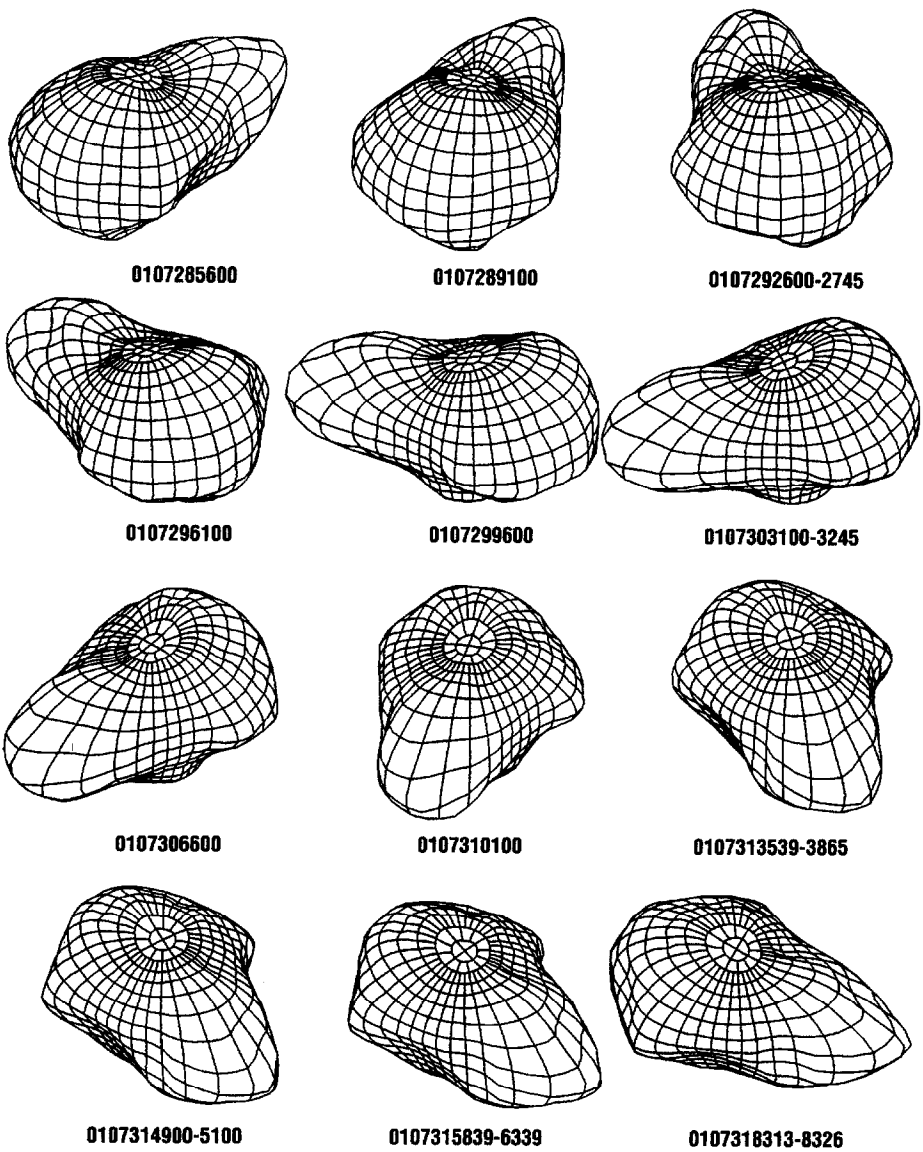

Figure 4. Latitude-longitude grids for the shape model, oriented to match the Galileo images.

Images of Gaspra were reprojected according to the shape model, and combined to create photomosaics (Figure 6). Figure 7 is a shaded relief map of the surface of Gaspra on a Morphographic Conformal projection, a conventional Stereographic projection modified for use with non-spherical objects. The shape which controls the projection is the three dimensional convex hull of the shape model. The outline of each map is the convex hull of the asteroid in the plane containing the long and

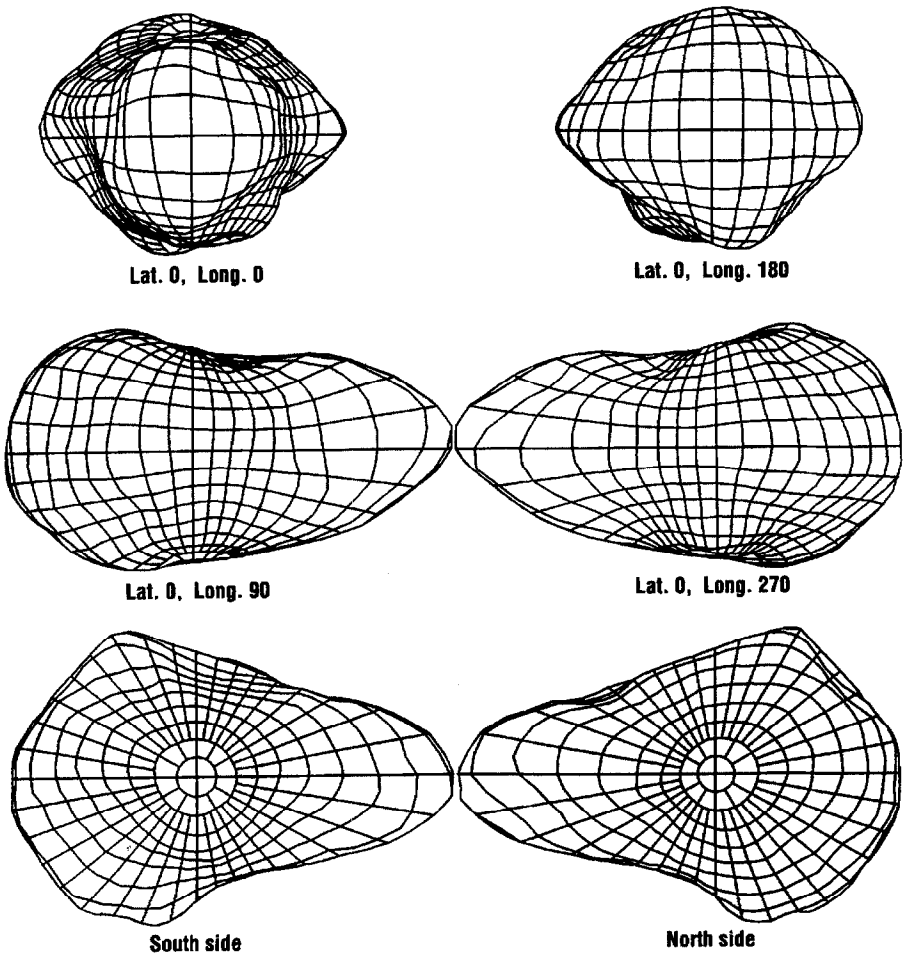

Figure 5. Latitude-longitude grids in six mutually perpendicular orientations.

rotation (short) axes. Several craters and distinct regions have been given names by the International Astronomical Union (1996). Those referred to in the text are identified in Figure 10.

In Figure 8 contours of the radius model are superimposed on the relief drawing. Radii are given in kilometres with a contour interval of 500 m. Elevations relative to a triaxial ellipsoid with axes of 16.0, 9.0 and 9.0 km are superimposed on relief in Figure 9. These are not identical to the dynamic heights of Thomas et al. (1994, Figure 6b), but the shape of the datum was selected so that the patterns of contours in Figure 9 and dynamic height contours are very similar. The dynamic height at any location is approximately half the elevation shown in Figure 9.

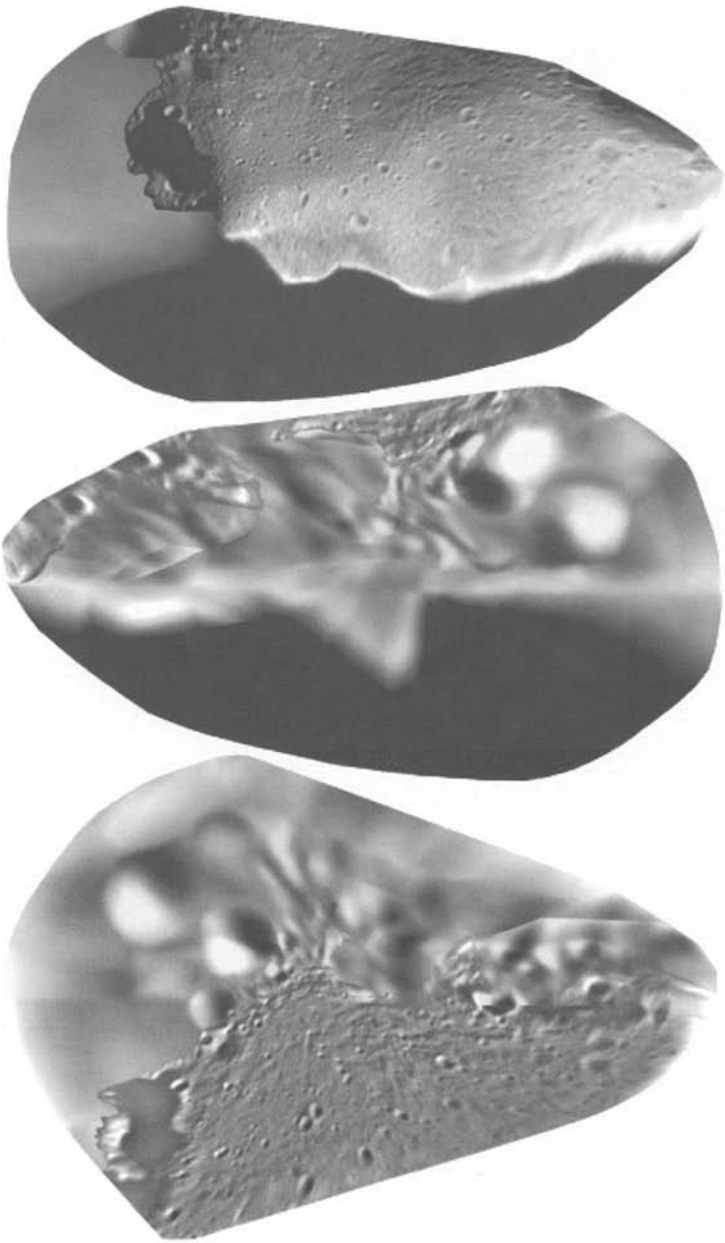

Figure 6. Photomosaics projected to the Morphographic Conformal projection of the convex hull of Gaspra. Mosaics are centred on the equator and 90° (top), the equator and 270° (middle) and the north pole (bottom).

Gaspra is very irregular in shape with several large nearly flat facets and a hemispherical blunt end, as shown in Figures 4 and 5. The equatorial outline is roughly triangular. Equatorial views centred at longitudes 90° and 270° indicate a

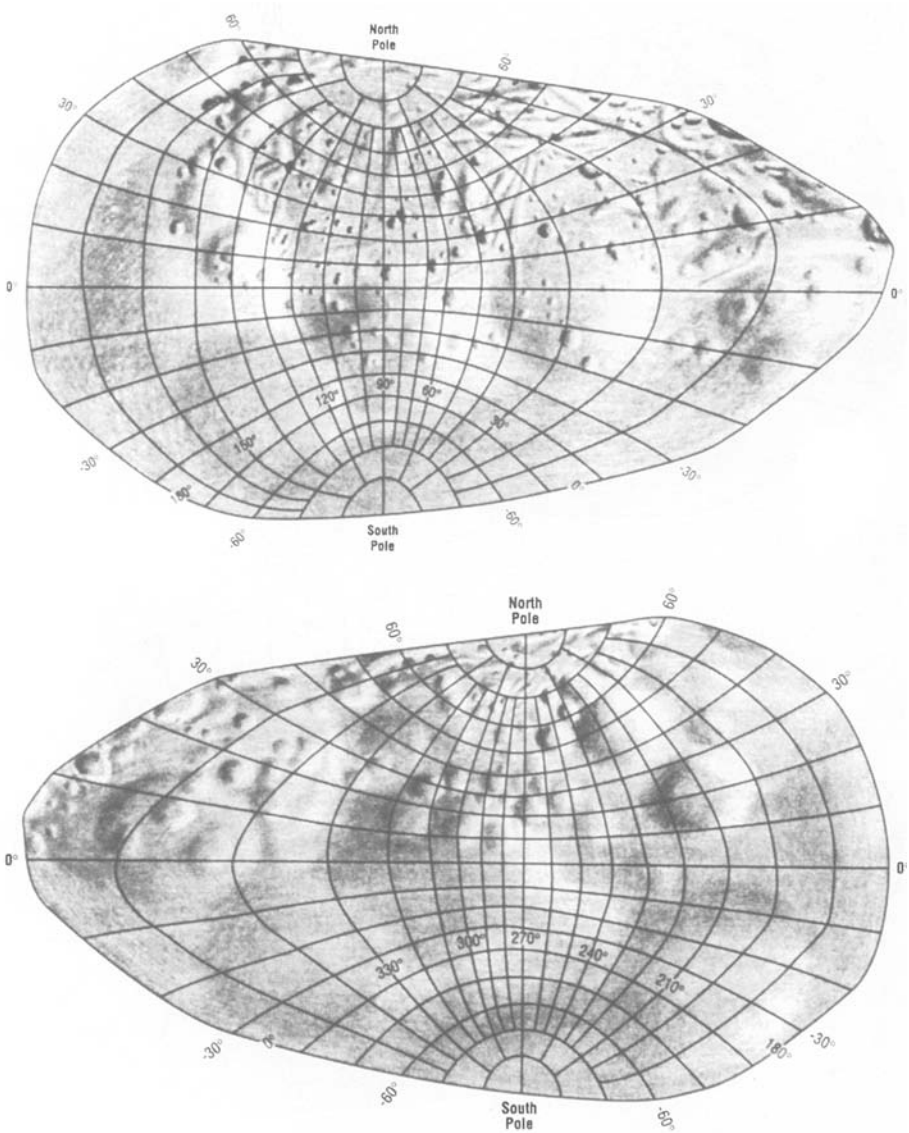

Figure 7. Shaded relief maps of Gaspra on the Morphographic Conformal Projection.

tapered body, more pointed along the 0° meridian than at 180°. The view along the long axis is extremely irregular.

The minimum radius in the model is 4.0 km at 65° N, 35° W. The maximum radius is 10.7 km at 5° N, 0° W. Uncertainties for both are about 300 m. The equatorial diameter of the model from 0° to 180° longitude is 18.1 km. From 90° to 270° the equatorial diameter is 10.0 km, and the polar diameter of the model is 9.0 km. The 90° to 270° diameter is reduced by the presence of two large

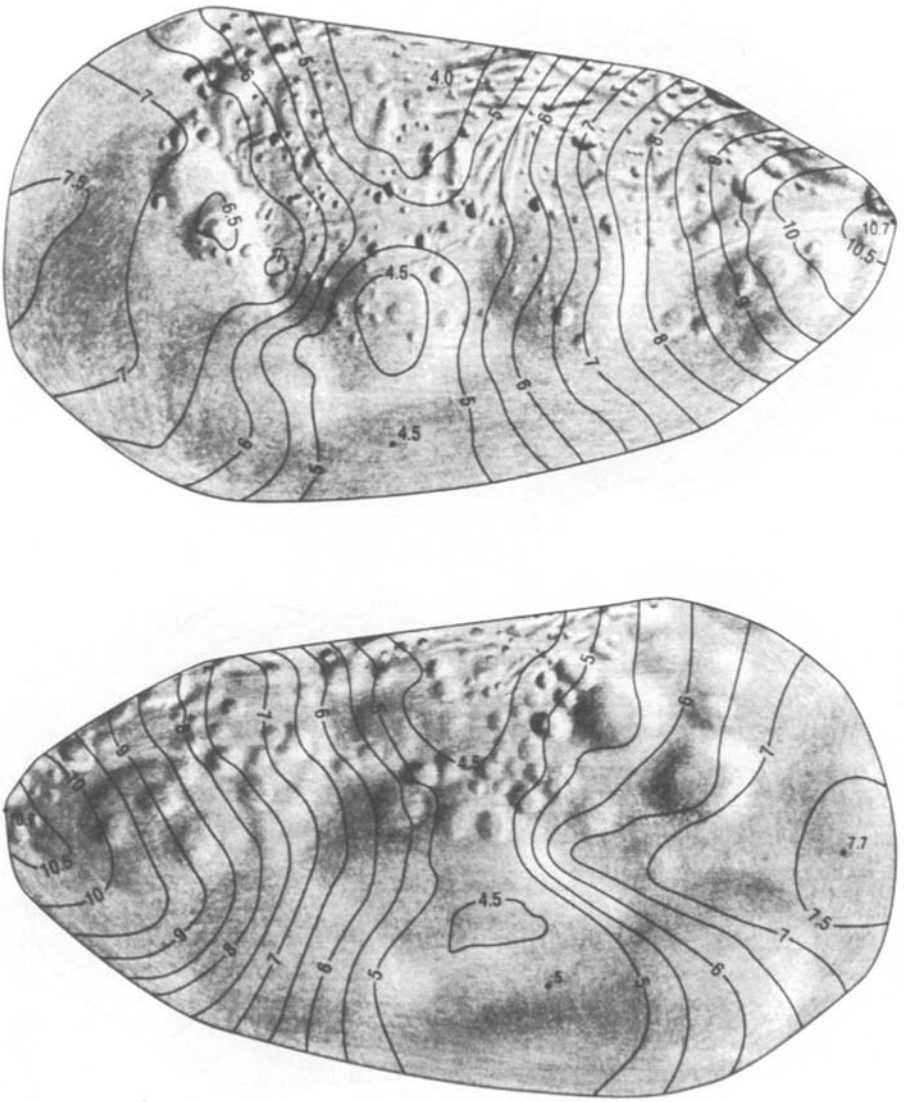

Figure 8. Shaded relief maps with contours of the radius model (km).

depressions opposite each other at these longitudes. The corresponding diameter of the convex hull is 11.0 km and the maximum width is 12.4 km. The volume of the model is 850 ± 200 km^3. This is about 10% smaller than the volume determined by Thomas et al. (1994), in part because it takes into account the revisions of Simonelli et al. (1995). The remaining volume discrepancy of some 70 km^3 is well within the estimated uncertainty. A triaxial ellipsoid with axes of 18.0, 10.5 and 8.8 km is a good fit to the overall shape and volume of the asteroid.

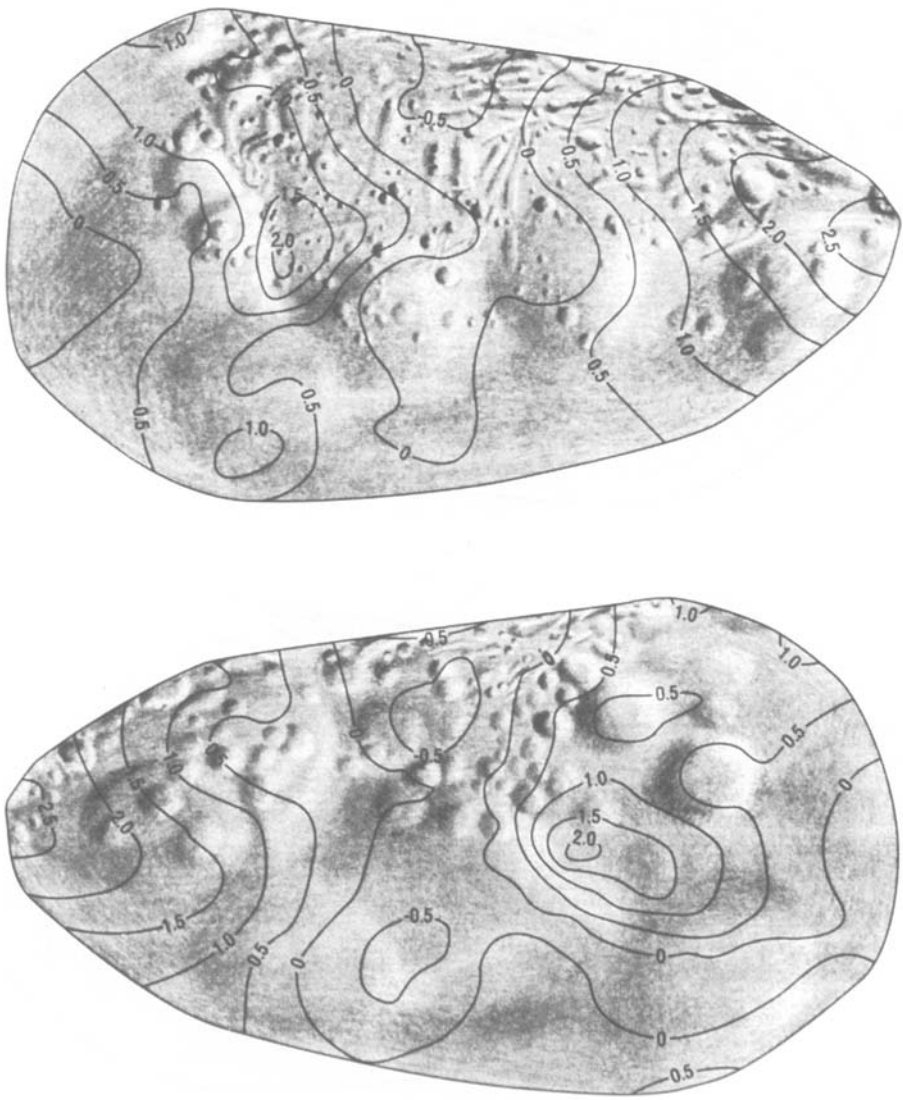

Figure 9. Shaded relief maps with contours of elevation relative to a 16 by 9 by 9 km ellipsoid.

5. Craters and Facets

The shape of Gaspra is dominated by large flat to slightly concave regions termed facets, of controversial origin. Some at least of these may be the remains of impact scars (Stooke, 1996). This interpretation has been discounted by Belton et al. (1992) and Chapman et al. (1996) because of the non-crateriform morphology of some and, more importantly, because of a prevailing expectation that Gaspra could not sustain such large impacts without disruption. Recent hydrocode modelling,

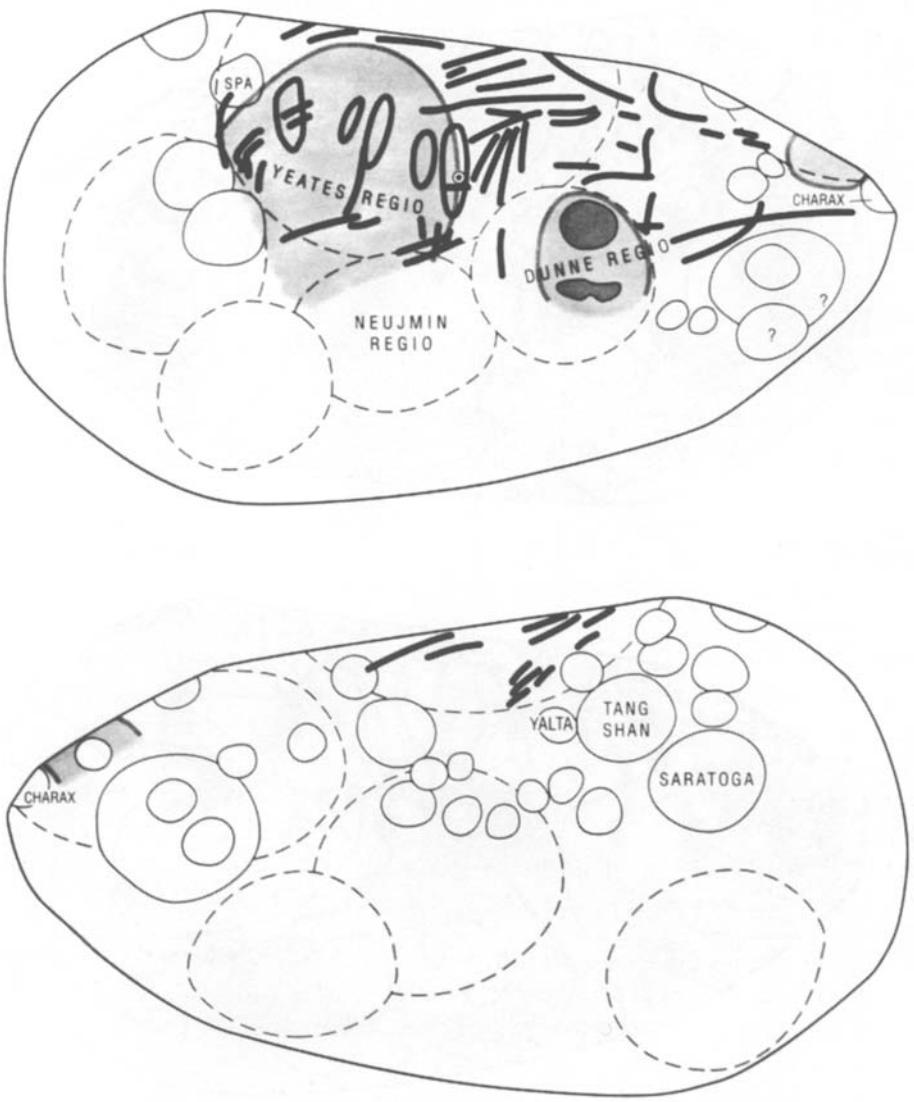

Figure 10. Geological sketch map of Gaspra. Dashed loops: facets; Solid loops: large craters; Heavy lines and elongated loops: grooves and troughs; Light shading: smooth material; Dark shading: darker material. Circle with central dot: possible block.

summarized by Greenberg et al. (1994), supports the notion that small bodies can survive impacts larger than previously thought. Thomas et al. (1994) noted that stereoscopic control points in Yeates Regio lay within 200 m of a plane over a 6 by 6 km area, and that the longitudes of normals to this and two other roughly planar regions were very similar. The implication may be that these facets are structurally

controlled, perhaps being formed as a parent body broke up along pre-existing fractures. Of course, facets of both types may coexist on a body.

Two observations suggest that Yeates Regio may represent an impact scar rather than a planar fracture surface. Grooves around much of the periphery of Yeates Regio curve slightly, giving the appearance of a discontinuous circumferential fracture zone. While not conclusive, this does suggest that the formation of Yeates Regio involved a radially symmetrical event or process. More importantly, a broad ridge near 40° N, 0° W, outside the area mapped by Thomas et al. (1994) as a plane, may be interpreted as part of the Yeates structure forming the rim of a gentle concavity. The subtle concavity is in fact faintly visible in the three multispectral image sequences prior to the highest-resolution view, but becomes invisible in high pass filtered versions. I interpret Yeates Regio as a very degraded impact scar about 7.5 km in diameter. Greenberg et al. (1994) also suggested this, but the impact scar described here includes part of their region 4 as well as Yeates Regio proper (their region 7).

Figure 10 shows several other facets as dashed loops. Nine are depicted, including Yeates, Neujmin and western Dunne Regiones. Another, well seen in intermediate resolution images is centred at 15° N, 345° W and was referred to as region 1 by Greenberg et al. (1994). A facet on the equator at 150° W is suggested by a flattened portion of the shape model and by shading in very low resolution images. Several facets with diameters of 4 or 5 km, lying south of the equator at longitudes 140°, 200° and 340° are suggested by flat or concave limb segments in various views. Other interpretations have included fewer facets, but these flat or concave limb segments certainly exist, and the most likely explanation is that at least some of them are facets like those seen more clearly. Even if only half of the nine features mapped here are remains of large craters, the implied cratering history of Gaspra must differ significantly from that suggested by Chapman et al. (1996):

> Facets cannot be successive crater-forming impacts; later scars would have destroyed earlier ones.... We expect that Gaspra was created by collisional fragmentation of a larger parent body... megaregolithic processes of reaccumulation and blanketing and/or shaking are evident, due to subsequent sub-catastrophic collisions. Gaspra's subdued craters peek through the effects of the last such collision.... Gaspra as we *know it* was created by collisional disruption and subsequently modified, perhaps more than once. Some hints about its next-to-last form may still be visible.

The "subdued craters" referred to here are faintly visible craters 500 to 1000 m across in Yeates Regio, not the larger facets. Greenberg et al. (1994) suggested instead that the facets are remnants of old craters, each successively subdued by more recent impacts.

Stooke (1996) introduced a terminology for large impacts on small bodies which is relevant to this discussion. Impacts are classified according to the effects they have on the body, scaled for size. An Order 1 impact catastrophically fragments

a body, and is responsible for the overall shape and size of individual fragments such as Gaspra. An Order 2 impact forms a facet, a crater with a diameter near the mean radius of the body itself, and erases or greatly subdues smaller features on a global scale by jolting the body severely. It is energetic enough to influence the global shape and rotation state of the body. An Order 3 impact shakes the whole body, redistributing debris near-globally but not influencing overall body shape or rotation. Order 4 impacts have only local effects, including the excavation of unweathered debris from beneath the regolith as reported by Helfenstein et al. (1994).

Gaspra's facets are interpreted by Chapman et al. (1996) as Order 1 fracture surfaces, subdued by later cratering. These authors assume that an Order 2 impact would reshape the surface on a global scale by massive spallation, possibly without leaving a recognizable crater, causing such severe damage that no earlier topography would survive. Greenberg et al. (1994) assume that Order 2 impacts can accumulate, each new Order 2 event forming its own facet or crater and smoothing earlier facets by shaking. Both authors interpret the numerous smaller craters as Order 3 and Order 4 features. Hydrocode simulations (Greenberg et al. (1994) seem to allow, and probably favour, the interpretation of facets as successive impact scars, and that interpretation is adopted here.

Belton et al. (1992), Carr et al. (1994) and Chapman et al. (1996) identified few craters over 1 km in diameter, and estimated surface ages of $300 \pm 100 \times 10^8$ years from crater frequency counts. These three studies were based on limited data. The first used only images 0107315839-6339, the earliest returned but having low resolution. The second and third studies involved counts made only in the region (Yeates Regio) seen in the highest resolution image sequence with optimal lighting and viewing geometries. Further analysis of all images leads me to a very different conclusion: craters 1 km in diameter or larger are fairly numerous, but the region seen at highest resolution is depleted in these craters relative to the rest of the surface. The age of Gaspra's surface is likely to be significantly greater than previously suggested.

Carr et al. (1994) and Chapman et al. (1996) recognized only one crater larger than 1 km across, Spa (diameter about 1.7 km), and noted the presence in low resolution images of two 3 km diameter craters at longitudes 210° and 225°. Others are visible, and still more are probable. One, at 50° N, 180° W, lies just beyond the terminator in the best images, but its southern rim protrudes beyond the terminator in 0107310100. It is about 1.5 km in diameter. Several craters of similar size lying around the two 3 km craters are hinted at by faint shadings on the disk in that same image and in 0107306600. There is one 2 km crater, and possibly a second degraded example about 3 km across, near 40° N, 330° W. That region is partly in shadow in the last 3 multispectral image sequences, and was referred to as a deep concavity by Helfenstein et al. (1994, Figure 9). A crater about 3.5 km across but apparently of very low relief, is centred at 5° N, 345° W. It can be seen faintly throughout the imaging coverage of the area, and its northeastern

rim forms the "smile" feature referred to by Greenberg et al. (1994, Figure 3). Those authors interpreted this ridge as a possible central peak of the larger facet in which it lies, but such structures would not be expected on an object the size of Gaspra. As discussed below, this region is one of two rotational leading surfaces on Gaspra which might accumulate impact ejecta, possibly accounting for the subdued topography. A subdued crater about 2.5 km across at 5° S, 5° W is faintly visible at high sun in sequence 0107313539-3865, and contains shadow in 0107310100 where it is near both the limb and the terminator. On its southern rim at 100 south, 5° W, a symmetrical indentation on the limb in the last few views of Gaspra hints at the presence of another crater about 1.5 km across. Finally, two craters each about 2 km in diameter are strongly suggested by the curving ridge protruding beyond the terminator at 20° N, 145° W in the highest resolution view, and are well shown in the reprojected mosaics in Figure 6.

In addition to these larger craters, several 1 km diameter craters are quite clearly visible along a ridge at 20° N, 300° W in images from 0107306600 to 0107316339. Several others in this size range are present in the region covered by the last few multispectral views, including examples at 20° N, 340° W and 50° N, 255° W.

These examples range from clearly identifiable craters seen at low resolution and thus not included in counts made only from the high resolution images, to highly uncertain but possible features. Even if only a few of the latter are accepted, it remains likely that the number of craters in the 1 to 4 km size range is much larger than had been considered previously. Given uncertainties in both existence and diameter of these poorly seen craters, no new cratering statistics are calculated here. However, the implication is that Gaspra's surface is older than previously thought, or to be more precise the elapsed time since the last large facet-forming (Order 2) impact is greater than previously thought. Gaspra's surface may record almost all Order 2 impacts since its formation at least 1×10^9 years ago (the mean lifetime assumed by Greenberg et al. (1994), and most of the Order 3 craters (1 to 4 km diameter) formed since the last Order 2 impact. Greenberg et al. (1994) invoked a much more recent Order 2 impact in order to account for the dearth of Order 3 craters, but the proposed additional craters make this unlikely event unnecessary.

The sparse cratering reported by previous authors remains an accurate observation to the extent that it refers to a specific area, almost wholly limited to Yeates Regio. There are good grounds for thinking that this region is unusual. Topography in this region is for the most part extremely subdued. The 150° meridian between 55° and 90° N separates two areas with very different characteristics, very smooth to the east and rugged, cratered and grooved to the west. The difference is clearly visible in the highest resolution view (Figure 1). The smooth terrain extends throughout Yeates Regio to the equatorial ridge separating it from Neujmin Regio, and east to about longitude 40° where the surface becomes pervasively grooved. Within Yeates are numerous subdued depressions widely regarded as being mantled or degraded impact craters (e.g. Chapman et al., 1996), and similarly subdued

and unusually wide grooves or linear depressions (Stooke, submitted). Both classes of feature suggest the presence of a thicker or more mobile regolith in this region. Since this area is one of Gaspra's rotational leading surfaces, as described for 243 Ida by Geissler et al. (1994), it would tend to sweep up ejecta from distant craters. It also lies on a fairly steep slope in the dynamic heights map of Thomas et al. (1994, Figure 6). Thus material might preferentially collect in this region, and be somewhat more mobile and susceptible to impact jolting. The only other regions of Gaspra which are rotational leading surfaces on steep slopes are Neujmin Regio, which is viewed very obliquely, and the large facet centred at 15° N, 350° W. A small part of the latter region on the prime meridian near 15° N is seen at high resolution at the terminator in image 0107318313. It is unusually smooth compared with adjacent parts of the terminator. This may also be a location with an unusually thick regolith. A similarly smooth area on the equator at 25° W is on a steep slope, steeper in my model than in that of Thomas et al. (1994), but is on a rotational trailing surface. The smoothness may be in part due to the very high sun angle in this region, though areas very close to it seem noticeably rougher. Although this trailing surface would not sweep up additional regolith, whatever is present here would tend to creep downslope when jolted, erasing small craters. All three identified smooth surfaces are indicated in Figure 10.

The conclusion I draw from all these observations is that Yeates Regio is unusually lightly cratered compared with most of Gaspra, and that previous crater frequency studies based on counts in this area do not give a representative age for the whole surface. Fresh craters in Yeates Regio date from the last large Order 3 impact on Gaspra, which jolted the thick regolith enough to mobilize it, erasing or greatly subduing older craters, and also contributed more debris to be swept up by the surface in this region. That Order 3 crater is likely to be either one of the 3 km craters near longitude 220°, or a similar crater on the unseen southern portion of Gaspra.

6. Blocks

Lee et al. (1996) describe blocks on Ida and suggest that blocks up to 70 m in diameter might be expected on Gaspra, but that blocks this size would be barely detectable in Galileo images. They indicate that a few candidates exist but do not identify them. The best such candidate would appear to be located at 31° N, 47° W at the eastern edge of Yeates Regio. It appears in image 0107318326 as a single bright pixel and a single dark pixel with contrast and orientation appropriate for this interpretation. The identification cannot be considered definitive because of the small size. If the apparent block is real it would be 60 ± 25 m in diameter. It is plotted on Figure 10. Several other possible blocks are visible in the two best images, mostly in the areas lacking the thicker regolith described here, but in all cases alternative interpretations such as crater rims are equally plausible.

7. Linear Features

Stooke (submitted) describes the system of grooves, ridges and crater chains which cross the surface of Gaspra. Extending the mapping of Belton et al. (1992) and Veverka et al. (1994b), that paper identifies two sets of lineaments, each possibly divisible into two subsets. One set is roughly parallel with the long axis of Gaspra, the other roughly perpendicular to it. These features are interpreted as the surface expressions in regolith of deep fractures, possibly joints originating from release of stress as Gaspra was excavated from a parent body by catastrophic impact. Drainage of regolith into fractures, including joints opened by impact jolting, is the preferred mechanism for groove or crater chain formation. As previously noted by Thomas et al. (1994), the extent and pattern of lineaments imply a monolithic interior rather than a binary or rubble pile structure.

8. Colour and Albedo Features

Belton et al. (1992) and Helfenstein et al. (1994) noted the presence in certain locations of "fresher" material, apparently less affected by a form of "space weathering" than most of Gaspra's surface. This weathering process has the effect of reducing the depth of the 1×10^{-6} m absorption band and slightly darkening and reddening the regolith. The brighter, bluer "fresh" material occurs predominantly on ridge crests, particularly around small craters on the ridges. The favoured interpretation is that the regolith is thinner on dynamic highs because of downslope movement driven by Order 3 impact jolting. The regolith gathers downslope in the facets, forming thicker deposits. Later small (order 4) craters penetrate the thin regolith on ridges, bringing unweathered material to the surface. Similar craters on facets rarely penetrate the thicker regolith to excavate unweathered material. This model is entirely consistent with the cratering interpretation presented here.

Fresher material is particularly prominent on the ridge between Yeates and Neujmin Regiones. A 250 m diameter crater at 5° N, 105° W (Belton et al., 1992, Figure 6a) displays perhaps the freshest signature of any part of Gaspra. The crater appears to lack a raised rim, possible evidence of having formed in a mechanically unusual area. A prominent 750 m diameter crater at 25° N, 0° W, on the rim of a facet, is also surrounded by fresh material. A ridge running down the 355° meridian at 60° N may have fresh material on its western slope, perhaps mobilized by a fresh crater at its crest. A few other locations of fresh material are indicated by Helfenstein et al. (1994, Figure 8).

Apart from these bright markings, one or possibly two dark markings, not previously described, are also visible in southern Dunne Regio in the last two imaging sequences. The most obvious is an irregular patch 500 by 1000 m across, perhaps subdivided into two lobes, at 7° S, 28° W. It shows clearly in both sets of images and has no obvious relief on or near it, although the very high sun would

make this difficult to see. Less certain is a faint dark halo, about 1 km across, around a 300 m diameter crater at 9° N, 26° W. This area seems redder and darker than the average for Gaspra in Figure 6 of Belton et al. (1992), although this may reflect errors in photometric correction for slope in their preliminary shape model. Both dark markings may reflect differences in photometric function (hence surface roughness) as well as or rather than albedo. Both are within the smooth deposit shown in Figure 10 which was discussed above. Some unusual property of impacts in the postulated deeper or more mobile regolith may be responsible. If they are real, similar anomalous areas may be masked by shadow in the lower sun regions of Yeates Regio. I note that similar dark markings are visible in a smooth deposit on the inner eastern wall of Vienna Regio on Ida.

9. Conclusions

More of the cratering history of Gaspra may be preserved on its surface than has been suggested by previous studies. Facets have probably accumulated since the formation of Gaspra, and should help constrain the age of that event. Craters 1 to 4 km in diameter have accumulated since the last facet-forming impact and thus date that event. Limitations of the imaging data will hinder attempts to derive that date. Small craters in Yeates Regio, which is probably mantled with a thicker or more mobile regolith than the average for Gaspra, may date the last crater large enough to shake the whole body, probably 3 or 4 km across. Three smooth deposits are identified, all on steep dynamic slopes, two on rotational leading surfaces, and all probably having thicker or more mobile regoliths. Grooves form two sets, roughly perpendicular to each other and apparently reflecting a fracture or jointing pattern in a monolithic interior. Bright material is associated with ridges, as previously noted, and one or perhaps two dark patches in Dunne Regio occur in a smooth deposit on a steep slope. A possible block about 60 m across has been identified.

Acknowledgements

This work was supported by the Natural Sciences and Engineering Research Council of Canada. I thank D. Mercer for help with the illustrations, D. Shillington for assistance with the manuscript, C. Woods for providing facilities for mapping, and J. Eligh for preliminary work on the Gaspra photomosaics.

References

Belton, M. J. S., Veverka, J., Thomas, P., Helfenstein, P., Simonelli, D., Chapman, C., Davies, M. E., Greeley, R., Greenberg, R., Head, J., Murchie, S., Klaasen, K., Johnson, T. V., McEwan, A., Morrison, D., Neukum, G., Fanale, F., Anger, C., Carr, M. and Pilcher, C.: 1992, *Science* **257**, 1647–1652.

Carr, M. H., Kirk, R. L., McEwan, A., Veverka, J., Thomas, P., Head, J. W., and Murchie, S.: 1994, *Icarus* **107**, 61–71.

Chapman, C. R., Veverka, J., Belton, M. J. S., Neukum, G., and Morrison, D.: 1996, *Icarus* **120**, 231–245.

Cheeseman, P., Kanefsky, R., Stutz, J., and Kraft, R.: 1994, *Lunar and Planetary Science XXV*, Lunar and Planetary Institute, Houston, Texas, pp. 241–242.

Geissler, P., Petit, J.-M., and Greenberg, R.: 1994, *Lunar and Planetary Science XXV*, Lunar and Planetary Institute, Houston, Texas, pp. 411–412.

Greenberg, R., Nolan, M. C., Bottke, W. F., and Kolvoord, R. A.: 1994, *Icarus* **107**, 84–97.

Helfenstein, P., Veverka, J., Thomas, P. C., Simonelli, D. P., Lee, P., Klaasen, K., Johnson, T. V., Breneman, H., Head, J. W., Murchie, S., Fanale, F., Robinson, M., Clark, B., Granahan, J., Garbeil, H., McEwan, A. S., Kirk, R. L., Davies, M. E., Neukum, G., Mottola, S., Wagner, R., Belton, M., Chapman, C., and Pilcher, C.: 1994, *Icarus* **107**, 37–60.

International Astronomical Union: 1996. *Proceedings of the 22nd General Assembly, The Hague, 1994*, in I. Appenzaller (ed.), Transactions of the I.A.U., v. XXIIB, 1994, pp. 225–231.

Lee, P., Veverka, J., Thomas, P. C., Helfenstein, P., Belton, M. J. S., Chapman, C. R., Greeley, R., Pappalardo, R. T., Sullivan, R., and Head, J. W.: 1996, *Icarus* **120**, 87–105.

Simonelli, D. P., Veverka, J., Thomas, P. C., Helfenstein, P., and Belton, M. J. S.: 1995, *Icarus* **114**, 387–402.

Stooke, P. J.: 1996, *Lunar and Planetary Science XXVII*, pp. 1281–1282.

Stooke, P. J.: forthcoming, 'Topography and Geology of Hyperion', *Earth Moon and Planets*, in press.

Stooke, P. J. and Lumsdon, M. P.: 1993, *Earth, Moon and Planets* **62**, 223–237.

Thomas, P. C., Veverka, J., Simonelli, D., Helfenstein, P., Carcich, B., Belton, M. J. S., Davies, M. E., and Chapman, C.: 1994, *Icarus* **107**, 23–36.

Veverka, J., Belton, M., Klaasen, K., and Chapman, C.: 1994a, *Icarus* **107**, 2–17.

Veverka, J., Thomas, P., Simonelli, D., Belton, M. J. S., Carr, M., Chapman, C., Davies, M. E., Greeley, R., Greenberg, R., Head, J., Klassen, K., Johnson, T. V., Morrison, D., and Neukum, G.: 1994b, *Icarus* **107**, 72–83.